J|A|C|S
ARTICLES
Published on Web 01/11/2006

# Determination of Equilibrium Constants for Atom Transfer Radical Polymerization

Wei Tang, Nicolay V. Tsarevsky, and Krzysztof Matyjaszewski*

*Contribution from the Center for Macromolecular Engineering, Department of Chemistry, Carnegie Mellon University, 4400 Fifth Avenue, Pittsburgh, Pennsylvania 15213*

Received September 2, 2005; E-mail: km3b@andrew.cmu.edu

***Abstract:*** Atom transfer radical polymerization (ATRP) equilibrium constants ($K_{ATRP}$) were determined using modified Fischer's equations for the persistent radical effect. The original Fischer's equations could be used only for low conversion of $Cu^{I}$ to $X-Cu^{II}$ and consequently for relatively low values of $K_{ATRP}$. At higher conversion to $X-Cu^{II}$ (>10%) and for larger values of $K_{ATRP}$ (>$10^{-7}$), modified equations that take into account the changes in catalyst and initiator concentrations should be used. The validity of new equations was confirmed by detailed kinetic simulations. UV−vis spectrometric and GC measurements were used to follow the evolution of $X-Cu^{II}$ species and the initiator concentration, respectively, and to successfully determine values of $K_{ATRP}$ for several catalysts and alkyl halides. The effect of structure on reactivities of ATRP components is presented.

## Introduction

Atom transfer radical polymerization (ATRP) is one of the most successful controlled/living radical polymerization (CRP) techniques and has been employed to produce many well-defined functional (co)polymers with predefined architecture.[1,2] ATRP is based on dynamic equilibration between dormant and active species catalyzed by redox active transition-metal complexes, such as Cu coordinated to various N-based ligands.[3−7] Radicals are formed from dormant alkyl halides (RX) by activation with $Cu^{I}$ species ($k_{act}$), after which they can either self-terminate ($k_t$), be deactivated by reaction with the $X-Cu^{II}$ species ($k_{deact}$), or propagate in the presence of a monomer ($k_p$).

The degree of control in ATRP is strongly affected by the position of the equilibrium ($K_{ATRP} = k_{act}/k_{deact}$) and by all rate constants. $K_{ATRP}$ depends on the solvent, temperature, monomer (i.e., structures of RX and $R^{\bullet}$), and structure of the Cu species. Several studies have reported measurements of kinetic and thermodynamic parameters in model and macromolecular systems.[3,8−22]

There are two general methods to determine the value of $K_{ATRP}$. First, $K_{ATRP}$ can be determined from polymerization kinetics, when an excess of the $X-Cu^{II}$ species is used and the concentration of all other species does not change significantly, provided that values of $k_p$ are known.[23]

$$R_p = k_p[M][P^*] = k_p K_{ATRP}[M][I]_0 \times [Cu^I]/[X-Cu^{II}] \quad (1)$$

Alternatively, $K_{ATRP}$ can be determined from the rate of formation of a persistent radical ($Y = [X-Cu^{II}]$) or from polymerization kinetics ($R = (1/k_p)(d\ ln[M]/dt)$), following the classic equations derived by Fischer and Fukuda for the persistent radical effect (PRE).[24−26]

$$\begin{cases} Y = (6k_t K_{ATRP}^2 I_0^{\,2} C_0^{\,2})^{1/3} t^{1/3} \\ R = \left(\dfrac{K_{ATRP} I_0 C_0}{6k_t}\right)^{1/3} t^{-1/3} \end{cases} \quad (2)$$

* To whom correspondence should be addressed. Fax: 412-268-6897.

(1) *Handbook of Radical Polymerization*; Matyjaszewski, K., Davis, T. P., Eds.; Wiley-Interscience: Hoboken, 2002.
(2) Matyjaszewski, K.; Xia, J. *Chem. Rev.* **2001**, *101*, 2921−2990.
(3) Matyjaszewski, K.; Goebelt, B.; Paik, H.-j.; Horwitz, C. P. *Macromolecules* **2001**, *34*, 430−440.
(4) Haddleton, D. M.; Waterson, C.; Derrick, P. J.; Jasieczek, C. B.; Shooter, A. J. *Chem. Commun.* **1997**, 683.
(5) Wang, J.-S.; Matyjaszewski, K. *J. Am. Chem. Soc.* **1995**, *117*, 5614−15.
(6) Xia, J.; Matyjaszewski, K. *Macromolecules* **1997**, *30*, 7697−7700.
(7) Queffelec, J.; Gaynor, S. G.; Matyjaszewski, K. *Macromolecules* **2000**, *33*, 8629−8639.
(8) Chambard, G.; Klumperman, B.; German, A. L. *Macromolecules* **2000**, *33*, 4417−4421.
(9) Goto, A.; Fukuda, T. *Macromol. Rapid Commun.* **1999**, *20*, 633−636.
(10) Matyjaszewski, K. *J. Macromol. Sci., Pure Appl. Chem.* **1997**, *A34*, 1785−1801.
(11) Matyjaszewski, K. *Macromolecules* **2002**, *35*, 6773−6781.
(12) Matyjaszewski, K.; Nanda, A. K.; Tang, W. *Macromolecules* **2005**, *38*, 2015.
(13) Matyjaszewski, K.; Paik, H.-j.; Zhou, P.; Diamanti, S. J. *Macromolecules* **2001**, *34*, 5125−5131.
(14) Nanda, A. K.; Matyjaszewski, K. *Macromolecules* **2003**, *36*, 599−604.
(15) Nanda, A. K.; Matyjaszewski, K. *Macromolecules* **2003**, *36*, 1487−1493.
(16) Nanda, A. K.; Matyjaszewski, K. *Macromolecules* **2003**, *36*, 8222−8224.
(17) Ohno, K.; Goto, A.; Fukuda, T.; Xia, J.; Matyjaszewski, K. *Macromolecules* **1998**, *31*, 2699−2701.
(18) Pintauer, T.; Braunecker, W.; Collange, E.; Poli, R.; Matyjaszewski, K. *Macromolecules* **2004**, *37*, 2679.
(19) Pintauer, T.; McKenzie, B.; Matyjaszewski, K.; ACS Symposium Series 854; American Chemical Society: Washington, DC, 2003, 130.
(20) Pintauer, T.; Zhou, P.; Matyjaszewski, K. *J. Am. Chem. Soc.* **2002**, *124*, 8196−8197.
(21) Tang, W.; Nanda, A. K.; Matyjaszewski, K. *Macromol. Chem. Phys.* **2005**, *206*, 1171−1177.
(22) Tsarevsky, N. V.; Pintauer, T.; Matyjaszewski, K. *Polym. Prepr.* **2004**, *45*(1), 1067.
(23) Matyjaszewski, K.; Patten, T. E.; Xia, J. *J. Am. Chem. Soc.* **1997**, *119*, 674−680.
(24) Zhang, H.; Klumperman, B.; Ming, W.; Fischer, H.; van der Linde, R. *Macromolecules* **2001**, *34*, 6169−6173.
(25) Fischer, H. *Chem. Rev.* **2001**, *101*, 3581.
(26) Goto, A.; Fukuda, T. *Prog. Polym. Sci.* **2004**, *29*, 329−385.


**10.1021/ja0558591 CCC: $33.50** 

***Scheme 1***

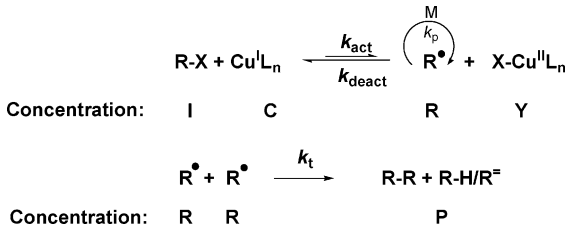


The symbols in eq 2 are clarified in Scheme 1. It should be noted that eq 2 was slightly modified by using $2k_t$ instead of $k_t$ because two transient radicals are consumed in one single termination step.[1,27] For consistency, all other equations derived by Fischer and Fukuda were modified accordingly. This method of determination of $K_{ATRP}$ is especially useful for model systems where the values of $k_t$ are diffusion controlled (in the range of $k_t \sim 2.5 \times 10^9$ $M^{-1}$ $s^{-1}$).[28,29] This procedure is less applicable when polymeric ATRP initiators are used because the termination rate constant is chain-length dependent.[30−32]

In this paper, we report a procedure for the determination of $K_{ATRP}$ using the classic Fischer's approach which, however, failed for large values of $K_{ATRP}$ when significant amounts of X−$Cu^{II}$ were formed. Therefore, we derived new equations for these systems, which were successfully tested using kinetic simulations. They also gave a deeper insight into why Fischer's original equations have limited validity. The newly determined $K_{ATRP}$ values helped to correlate structures of the ATRP reagents with their reactivities.

## Experimental Section

**Materials.** Ethyl 2-bromoisobutyrate (EtBriB, 99%, Aldrich), bromopropionitrile (BrPN, 97%, Aldrich), 1-(bromoethyl)benzene (PEBr, 98%, Aldrich), benzyl bromide (BzBr, 98%, Aldrich), methyl DL-2-bromopropionate (MBrP, 99%, Acros), methyl chloroacetate (MClAc, 99+%, Aldrich), acetonitrile (MeCN, Aldrich, 99+%, HPLC grade), *N*,*N*,*N*′,*N*″,*N*″-pentamethyldiethylenetriamine (PMDETA) (99+%, Aldrich), 2,2′-bipyridine (bpy) (99%, Aldrich), $Cu^{I}Cl$ (99.995%, Aldrich), and $Cu^{I}Br$ (99.999%, Aldrich) were used as received. Tris[(2-pyridyl)-methyl]amine (TPMA) was synthesized according to a literature procedure.[33] Prior to use, all liquid reagents and the solvents were deoxygenated by bubbling with nitrogen for at least 2 h.

**General Procedure for the Determination of Equilibrium Constants.** A portion of 7.17 mg (0.05 mmol) of $Cu^{I}Br$ or 4.95 mg (0.05 mmol) of $Cu^{I}Cl$ was added to a Schlenk flask joined to a quartz UV cuvette, and then the Schlenk flask was carefully sealed. The flask was evacuated and back-filled with $N_2$ five times. A portion of 10 mL of MeCN was added to the flask via a nitrogen-purged syringe through the side arm. PMDETA (10.4 $\mu$L, 0.05 mmol) was then added through the side arm of the flask via a $N_2$-purged microsyringe. The contents were stirred until a colorless solution was obtained. The corresponding alkyl halide (purged with nitrogen, 0.05 mmol ∼ 0.1 mmol) was then transferred to the Schlenk flask via a $N_2$-purged microsyringe. The absorbance at a wavelength corresponding to the $\lambda_{max}$ of the generated X−$Cu^{II}$ complex was monitored at timed intervals. The concentration of the deactivator generated in the system was calculated using values of the extinction coefficients for the $Cu^{II}$ complexes determined separately. The spectroscopic measurements were performed on a Lambda 900 (Perkin-Elmer) UV/vis/NIR spectrometer. Other combinations of alkyl halides and $Cu^{I}$ complexes were studied in a similar fashion.

The experimental procedure used to determine the values of $K_{ATRP}$ by GC is similar to that in our previous publication detailing the determination of $k_{act}$.[12]

**Simulation.** The Predici program (version 5.0) was used for kinetic modeling.[34,35] It employs an adaptive Rothe method as a numerical strategy for time discretization. Concentrations of all species can be followed. Calculations were performed on a personal computer and took approximately 3−5 min to complete.

## Results and Discussions

**Determination of $K_{ATRP}$ by UV−Vis Spectrometry Using Fischer's Equation for PRE. A. Lower Values of $K_{ATRP}$.** The equilibrium constant for ATRP could be determined using the analytical solution proposed by Fischer for the persistent radical effect.[36,37] In the absence of a monomer, the ATRP equilibrium (Scheme 1) simplifies to three elementary reactions: activation ($k_{act}$), deactivation ($k_{deact}$), and termination ($k_t$). In this case, the rate of formation of the deactivator (the persistent radical, X−$Cu^{II}$ species) and the rate of loss of the generated transient radical are given by the following expressions:

$$\begin{cases} \dfrac{dR}{dt} = k_{act}IC - k_{deact}RY - 2k_tR^2 \\ \dfrac{dY}{dt} = k_{act}IC - k_{deact}RY = \dfrac{dR}{dt} + 2k_tR^2 \end{cases} \quad (3)$$

The two coupled differential equations have been solved analytically by Fischer.[36] He concluded that the increase of concentration of the deactivator (Y) should be a linear function of $t^{1/3}$, and the loss of the transient radical (R) should be proportional to $t^{-1/3}$ (eq 2). For equimolar concentrations of ATRP initiator and catalyst, this dependence should be valid in the time interval defined by eq 4, if eq 5 is also fulfilled.[25,36] For nonequimolar conditions, both equations should be modified, as shown in Appendix I in the Supporting Information.

$$\frac{4\sqrt{k_t}K_{ATRP}}{3I_0k_{act}^{3/2}} < t < \frac{1}{6K_{ATRP}^2k_tI_0} \quad (4)$$

$$K_{ATRP} < k_{deact}/4k_t \quad (5)$$

Thus, in the above time regime (eq 4), a plot of Y (i.e., [X−$Cu^{II}$]) vs $t^{1/3}$ can be used to determine $K_{ATRP}$, provided that a value of $k_t$ for the radical termination reaction is known. The termination of two small radicals, without any unusual steric effects, is governed by diffusion limits ($k_t = 2.5 \times 10^9$ $M^{-1}$ $s^{-1}$ at ambient temperature in most organic solvents).[28,29] Some variation in $k_t$ will introduce small errors in the overall analysis.

To test the accuracy of the analytical solution for the persistent radical effect (eq 2) in determining $K_{ATRP}$, a kinetic simulation

(27) Buback, M.; Egorov, M.; Gilbert, R. G.; Kaminsky, V.; Olaj, O. F.; Russell, G. T.; Vana, P.; Zifferer, G. *Macromol. Chem. Phys.* **2002**, *203*, 2570−2582.
(28) Fischer, H.; Henning, P. *Acc. Chem. Res.* **1987**, *20*, 200−206.
(29) Fischer, H.; Radom, L. *Angew. Chem., Int. Ed.* **2001**, *40*, 1340−1371.
(30) Barner-Kowollik, C.; Buback, M.; Egorov, M.; Fukuda, T.; Goto, A.; Olaj, O. F.; Russell, G. T.; Vana, P.; Yamada, B.; Zetterlund, P. B. *Prog. Polym. Sci.* **2005**, *30*, 605−643.
(31) Shipp, D. A.; Matyjaszewski, K. *Macromolecules* **2000**, *33*, 1553−1559.
(32) Shipp, D. A.; Matyjaszewski, K. *Macromolecules* **1999**, *32*, 2948−2955.
(33) Tyeklar, Z.; Jacobson, R. R.; Wei, N.; Murthy, N. N.; Zubieta, J.; Karlin, K. D. *J. Am. Chem. Soc.* **1993**, *115*, 2677−89.
(34) Wulkow, M. *Macromol. Theory Simul.* **1996**, *5*, 393−416.
(35) Lutz, J.-F.; Matyjaszewski, K. *Macromol. Chem. Phys.* **2002**, *203*, 1385−1395.
(36) Fischer, H. *J. Polym. Sci., Part A: Polym. Chem.* **1999**, *37*, 1885−1901.
(37) Ohno, K.; Tsujii, Y.; Miyamoto, T.; Fukuda, T.; Goto, M.; Kobayashi, K.; Akaike, T. *Macromolecules* **1998**, *31*, 1064−1069.

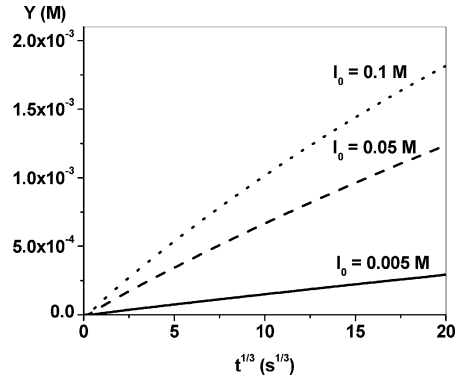


***Figure 1.*** Simulation of the formation of X−Cu$^{II}$ to determine $K_{ATRP}$ via Fischer's equation (Y vs $t^{1/3}$): $k_{act} = 1.0\ M^{-1}\ s^{-1}$, $k_{deact} = 5.0 \times 10^7\ M^{-1}\ s^{-1}$, $k_t = 2.5 \times 10^9\ M^{-1}\ s^{-1}$, $C_0 = 0.005$ M, $I_0 = 0.1$ M (dotted line), 0.05 M (broken line), and 0.005 M (solid line).

***Table 1.*** Initial, Final, and Least-Square Fit of $K_{ATRP}$ from Figure 1[a]

| | $C_0$ (M) | $I_0$ (M) | $K_{ATRP}$ | $K_{ATRP}$ (initial) | $K_{ATRP}$ (final) | $K_{ATRP}$ (av) |
|---|---|---|---|---|---|---|
| dotted line | 0.005 | 0.1 | $2.0 \times 10^{-8}$ | $2.31 \times 10^{-8}$ | $1.07 \times 10^{-8}$ | $1.49 \times 10^{-8}$ |
| broken line | 0.005 | 0.05 | $2.0 \times 10^{-8}$ | $2.36 \times 10^{-8}$ | $1.30 \times 10^{-8}$ | $1.65 \times 10^{-8}$ |
| solid line | 0.005 | 0.005 | $2.0 \times 10^{-8}$ | $2.37 \times 10^{-6}$ | $1.69 \times 10^{-8}$ | $1.88 \times 10^{-8}$ |

[a] The $K_{ATRP}$ (initial), $K_{ATRP}$ (final), and $K_{ATRP}$ (av) were obtained by least-squares fitting for the first 20 points, the last 20 points, and the overall plot, respectively.

was conducted using Predici 5.0 kinetic simulation software.[38] The rate constants used in the simulations were $k_{act} = 1.0\ M^{-1}\ s^{-1}$, $k_{deact} = 5.0 \times 10^7\ M^{-1}\ s^{-1}$ ($K_{ATRP} = 2.0 \times 10^{-8}$), and $k_t = 2.5 \times 10^9\ M^{-1}\ s^{-1}$. Figure 1 shows the plot of the concentration of the X−Cu$^{II}$ complex (Y) vs $t^{1/3}$ for different initial concentrations of the Cu$^{I}$ complex ($C_0$) and alkyl halide ($I_0$). $K_{ATRP}$ values were calculated from the initial slopes ($K_{ATRP}$ (initial)), final slopes ($K_{ATRP}$ (final)), and least-squares fits of the whole data set available ($K_{ATRP}$ (av)) according to eq 2 (Table 1). The $K_{ATRP}$ values for low concentration of the initiator ($I_0$) were close to the real value of $2.0 \times 10^{-8}$. At higher $I_0$, and also when more Y was formed, these values became lower. In fact, no constant value of $K_{ATRP}$ could be observed for any of these systems.

Figure 2 shows the plot for Y ([X−Cu$^{II}$]) vs $t^{1/3}$ for an actual reaction between [Cu$^{I}$Br/PMDETA]$_0$ = 100 mM and [PEBr]$_0$ = 5 mM in MeCN at 22 °C. $K_{ATRP}$ calculated from the initial slope was $K_{ATRP} = 2.94 \times 10^{-8}$, but one can observe a progressively more pronounced curvature at longer reaction times. The equilibrium constant calculated from the final slope was $K_{ATRP}$ (final) $= 1.40 \times 10^{-8}$; if all the experimental points were used, a value of $K_{ATRP}$ (av) $= 2.06 \times 10^{-8}$ was determined.

**B. More Reactive Systems with Higher Values of $K_{ATRP}$.** An increased curvature in Fischer's plots was observed for faster reactions, for example, when EtBriB was used in the reaction with Cu$^{I}$Br/TPMA (Figure 3). This figure was obtained by following the reaction of an equimolar (5 mM) amount of reactants. The initial slope (probably measured before the quasi-equilibrium was established) gave a value of $K_{ATRP} = 2.53 \times 10^{-6}$. The final slope (which could be affected by side

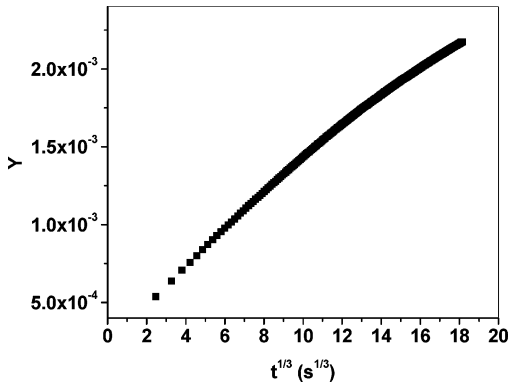


***Figure 2.*** Experimental determination of $K_{ATRP}$ via Fischer's equation (Y vs $t^{1/3}$): [Cu$^{I}$Br/PMDETA]$_0$ = 5 mM, [PEBr]$_0$ = 100 mM, in MeCN at 22 °C.

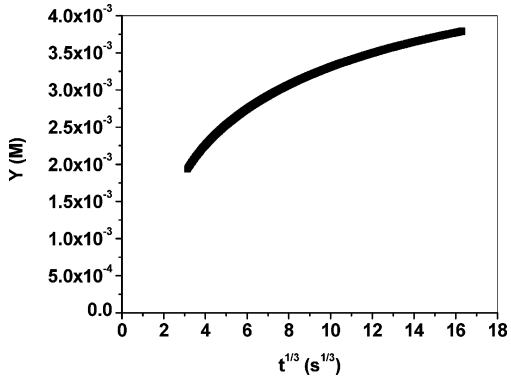


***Figure 3.*** Experiment for the determination of $K_{ATRP}$ via Fischer's equation (Y vs $t^{1/3}$): [Cu$^{I}$Br/TPMA]$_0$ = [EtBriB]$_0$ = 5 mM, in MeCN at 22 °C.

reactions) yielded a value of $K_{ATRP} = 1.38 \times 10^{-7}$. The least-squares fit of all data gave $K_{ATRP} = 3.35 \times 10^{-7}$.

Similar or even more pronounced curvatures were observed for all systems which involved more reactive ATRP reagents and proceeded to higher Cu$^{I}$ conversions. These observations prompted us to carry out another kinetic simulation because, for the simulation shown in Figure 1, a relatively small value of $K_{ATRP}$ ($2.0 \times 10^{-8}$) was used, and the reaction proceeded to low conversion of Cu$^{I}$ (<35% of $C_0$). Simulations were carried out for large values of $K_{ATRP}$ as well as for lower values of $K_{ATRP}$ over a longer reaction time, and both were driven to high Cu$^{I}$ conversion, as shown in Figure 4. In all cases, the plots of Y vs $t^{1/3}$ are nonlinear and curvature becomes easily detectable when the conversion of Cu$^{I}$ is higher than ~30%. The calculated $K_{ATRP}$ from the initial slope, the final slope, and the least-squares fit of all data is listed in Table 2.

According to Fischer's equation (eq 4), the plots should be straight over a very wide time range; i.e., $1.38\ s^{1/3} < t^{1/3} < 77.83\ s^{1/3}$ for $k_{act} = 1\ M^{-1}\ s^{-1}$, $I_0 = C_0 = 5$ mM, and $K_{ATRP} = 2 \times 10^{-7}$ (for the first system) and $0.39\ s^{1/3} < t^{1/3} < 49.03\ s^{1/3}$ for $k_{act} = 1\ M^{-1}\ s^{-1}$, $I_0 = 0.1$ M, $C_0 = 5$ mM, and $K_{ATRP} = 2 \times 10^{-8}$ (for the second system).[36,39]

The requirement (eq 5) proposed by Fischer for the validity of eq 2 is fulfilled for both systems: $k_{deact} = (k_{act}/K_{ATRP}) = 5 \times 10^6$ or $5 \times 10^7\ M^{-1}\ s^{-1}$ and $k_t = 2.5 \times 10^9\ M^{-1}\ s^{-1}$; i.e., $K_{ATRP}$ ($2 \times 10^{-8}$) is much lower than the ratio $k_{deact}/4k_t$ ($5 \times 10^{-4}$ or $5 \times 10^{-3}$, respectively).[25,36]

(38) Hungenberg, K. D.; Chen, C. C.; Zhang, F.; Wulkow, M.; Stubbe, G.; Nieken, U. *DECHEMA Monographien* **2001**, 137, (7th International Workshop on Polymer Reaction Engineering, 2001), 237−245.

(39) Fischer, H. *J. Am. Chem. Soc.* **1986**, *108*, 3925−7.

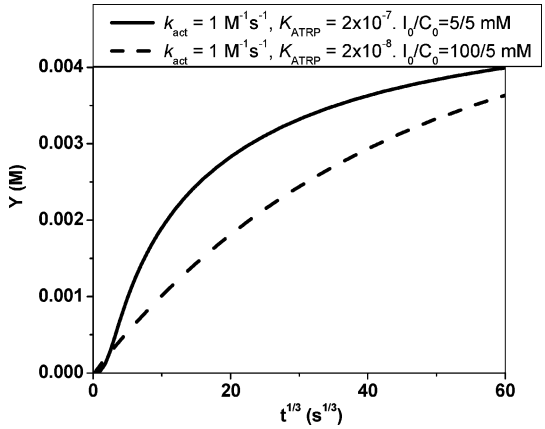


***Figure 4.*** Simulation for the determination of $K_{ATRP}$ via Fischer's equation (Y vs $t^{1/3}$) for a fast (solid line) and a slow (broken line) reaction proceeding to high conversion of $Cu^I$; $k_t = 2.5 \times 10^9$ $M^{-1}$ $s^{-1}$.

***Table 2.*** Initial, Final, and Least-Square Fit of $K_{ATRP}$ from Figure 4[a]

| | $k_{act}$ ($M^{-1}$ $s^{-1}$) | $K_{ATRP}$ | $K_{ATRP}$ (initial) | $K_{ATRP}$ (final) | $K_{ATRP}$ (av) |
|---|---|---|---|---|---|
| solid line | 1.0 | $2 \times 10^{-7}$ | $1.17 \times 10^{-6}$ | $1.05 \times 10^{-8}$ | $1.14 \times 10^{-7}$ |
| broken line | 1.0 | $2 \times 10^{-8}$ | $1.51 \times 10^{-8}$ | $9.12 \times 10^{-10}$ | $4.73 \times 10^{-9}$ |

[a] The $K_{ATRP}$ (initial), $K_{ATRP}$ (final), and $K_{ATRP}$ (av) were obtained by least-squares fitting for the first 20 points, the last 20 points, and the overall plot, respectively.

**C. Previous Derivations of PRE Equations.** Previous derivations of an persistent radical effect relied on the establishment of an equilibrium between active and dormant species. For nitroxide-mediated polymerization (NMP), the activation process is unimolecular, but for ATRP, activation involves the alkyl halide initiator ($I$) and the $Cu^I$ catalyst ($C$). Both Fischer and Fukuda assumed that the concentrations of the initiator and the catalyst changed insignificantly compared to their initial values:[26,36]

$$k_{deact}RY = k_{act}I_0C_0 \tag{6}$$

In eq 6, the deactivation rate ($R_{deact} = k_{deact}RY$) in ATRP or NMP is proposed to be equal to the initial rate of activation ($k_{act}I_0C_0$ in ATRP or $k_{act}I_0$ in NMP) and should remain constant throughout the time range defined by eq 4. Equation 6 can be rewritten as $K_{ATRP} = k_{act}/k_{deact} = (RY/I_0C_0)$, which suggests that $K_{ATRP}$ should only depend on the product of R and Y or that the product of R and Y should be constant over the stated time range in eq 4.

Figure 5 shows three different concentration ratios ($RY/IC$, $RY/I_0C$, and $RY/I_0C_0$) as well as the real $K_{ATRP}$ value ($2 \times 10^{-8}$) used in the simulated ATRP. It is clear that both the ratios $RY/I_0C_0$ and $RY/I_0C$ deviate from the real value of $K_{ATRP}$. This is observed even for the relatively slow reactions and for low conversion of $Cu^I$ to $X-Cu^{II}$ (<30%). On the other hand, $RY/IC$ approaches $K_{ATRP}$ after 10 s (when rates of activation and deactivation are balanced) and is then almost identical to the real $K_{ATRP}$ value. Therefore, for the derivation of correct equations describing evolution of Y and R, $K_{ATRP} = RY/IC$ should be used instead of $K_{ATRP} = RY/I_0C_0$.

**D. Derivation of New Equations for the Persistent Radical Effect.** On the basis of the above conclusions along with the stoichiometric requirement, i.e., $I_0 - I = C_0 - C = Y$, and the assumption $dY/dt \gg -dR/dt$, new equations were derived for Y as shown in eq 7 (detailed derivation is included in Appendix II of the Supporting Information).

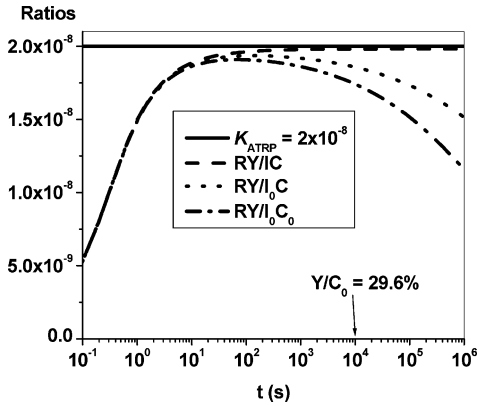


***Figure 5.*** Various concentration ratios obtained from Predici simulations using $K_{ATRP} = 2 \times 10^{-8}$, $k_{act} = 1$ $M^{-1}$ $s^{-1}$, and $k_t = 2.5 \times 10^9$ $M^{-1}$ $s^{-1}$. $I_0 = C_0 = 5$ mM.

For $C_0 \neq I_0$

$$\left(\frac{I_0C_0}{C_0 - I_0}\right)^2\left(\frac{1}{C_0^2(I_0 - Y)} + \frac{2}{I_0C_0(C_0 - I_0)}\ln\left(\frac{I_0 - Y}{C_0 - Y}\right) + \frac{1}{I_0^2(C_0 - Y)}\right) = 2k_tK_{ATRP}^2t + c'$$

$$\text{where } c' = \left(\frac{I_0C_0}{C_0 - I_0}\right)^2\left(\frac{1}{C_0^2I_0} + \frac{2}{I_0C_0(C_0 - I_0)}\ln\frac{I_0}{C_0} + \frac{1}{I_0^2C_0}\right) \tag{7}$$

Note that $2k_t$ was used in the derivation instead of $k_t$ because $R_t = 2k_tR^2$.

Thus, a new function $F(Y)$ (where Y is the only variable) can be used to calculate $K_{ATRP}$:

$$F(Y) = \left(\frac{I_0C_0}{C_0 - I_0}\right)^2\left(\frac{1}{C_0^2(I_0 - Y)} + \frac{2}{I_0C_0(C_0 - I_0)}\ln\left(\frac{I_0 - Y}{C_0 - Y}\right) + \frac{1}{I_0^2(C_0 - Y)}\right) \tag{8}$$

A plot of $F(Y)$ vs $t$ should be a straight line, and the equilibrium constant for the reaction can be calculated from the slope ($K_{ATRP} = \sqrt{\text{slope}/2k_t}$) with the intercept of $c'$.

An even simpler equation was derived for the equimolar case. For $C_0 = I_0$

$$\frac{C_0^2}{3(C_0 - Y)^3} - \frac{C_0}{(C_0 - Y)^2} + \frac{1}{C_0 - Y} = 2k_tK_{ATRP}^2t + c''$$

$$\text{where } c'' = \frac{1}{3C_0} \tag{9}$$

The function $F(Y)$ is now defined as

$$F(Y) = \frac{C_0^2}{3(C_0 - Y)^3} - \frac{C_0}{(C_0 - Y)^2} + \frac{1}{C_0 - Y} \tag{10}$$

and a plot $F(Y)$ vs $t$ should be a straight line; the equilibrium

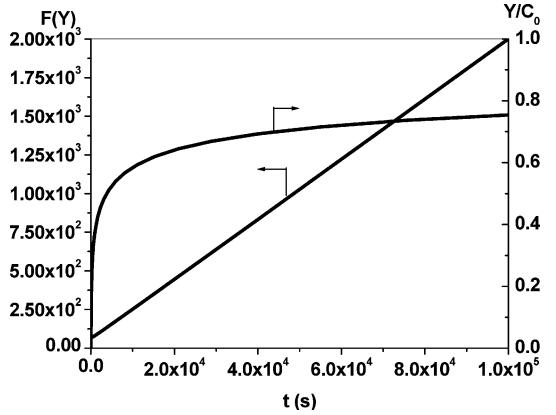


***Figure 6.*** Simulation for the determination of $K_{ATRP}$ via new equations ($F$(Y) vs $t$): $k_{act} = 1\ M^{-1}\ s^{-1}$, $k_t = 2.5 \times 10^9\ M^{-1}\ s^{-1}$, $K_{ATRP} = 2.0 \times 10^{-7}$, $I_0 = C_0 = 5$ mM, $K_{ATRP}$(calcd) $= 1.98 \times 10^{-7}$, intercept = 66.5 (entry 6 in Table 3).

constant can be calculated from the slope ($K_{ATRP} = \sqrt{\text{slope}/2k_t}$) with an intercept of $c''$.

**E. Simulations Using New Equations.** To test the validity of the new equations, a Predici simulation was carried out for a reaction with a relatively large $K_{ATRP}$ ($2 \times 10^{-7}$) under equimolar conditions, as shown in Figure 6. The plot of $F$(Y) vs $t$ is linear over a long reaction time and gives the value $K_{ATRP} = 1.98 \times 10^{-7}$, which is very close to the value of $K_{ATRP}$ used in the simulation. The intercept value equaled precisely the predicted one from eq 9 ($c'' = 66.5$). The simulations show that the new derived equations are valid over a very large range of reaction time (from seconds to essentially infinite time) and for a large range of activator conversion up to >95% (not shown in Figure 6).

It should be noted that for the same simulation conditions a constant curvature was observed using Fischer's equation (Y $\sim t^{1/3}$), as shown in Figure 4. Thus, Fischer's equations are never fully obeyed because neither $I$ nor $C$ is constant. Therefore, using these equations, it is not possible to determine precisely $K_{ATRP}$ because evolution of Y vs $t^{1/3}$ is never linear and changes continuously. At the very short time, the quasi-equilibrium is not yet established and, subsequently, the slope of the curve decreases due to the consumption of the initiator and the activator. This is illustrated by the various values of $K_{ATRP}$ (initial), $K_{ATRP}$ (final,) and $K_{ATRP}$ (av) shown earlier in Tables 1 and 2 and Figures 1−4.

Results of several other simulations for a constant $k_{act}$ and various $k_{deact}$ values are listed in Table 3 along with values of $K_{ATRP}$ calculated using the new equations. All values of $K_{ATRP}$ calculated from the slope of the plots are within 1−2% of those defined by $k_{act}/k_{deact}$. This indicates that eqs 7 and 9 are valid over a wide range of $K_{ATRP}$ values and for a broad range of reaction times. It should be noted that for very large values of $K_{ATRP}$ (approaching the limit defined in eq 5) the slopes still provide correct values of $K_{ATRP}$, but intercepts (shown in italics) start to deviate from the theoretical values. This is related to the time needed to establish the equilibrium which shifts the $F$(Y) function on the time scale (cf. Appendix III of Supporting Information).

**F. Reevaluation of Relatively Small Values of $K_{ATRP}$ Measured Previously via UV−Vis Spectrometry.** Two experiments shown previously in Figures 2 and 3 were reevaluated using the new equations. Figures 7 and 8 show the results using double-axes plots for the original PRE and newly derived equations.

As shown in Figure 7, the plot from Fischer's equation does not deviate significantly from linearity because the $K_{ATRP}$ for $Cu^IBr$/PMDETA with PEBr is small and the conversion of $Cu^I$ to $X-Cu^{II}$ is <50%. Regardless, it is difficult to determine the true value of $K_{ATRP}$ ($K_{ATRP}$ (initial) $= 2.94 \times 10^{-8}$, $K_{ATRP}$ (final) $= 1.40 \times 10^{-8}$, $K_{ATRP}$ (av) $= 2.06 \times 10^{-8}$). However, the plot becomes perfectly straight using the new equation and gives $K_{ATRP} = 3.27 \times 10^{-8}$.

***Table 3.*** Simulation of Various $K_{ATRP}$ Values via the New Equations[a]

| no. | $k_{act}$ ($M^{-1}s^{-1}$) | $k_{deact}$ ($M^{-1}s^{-1}$) | $I_0/C_0$ (mM) | $K_{ATRP}$ (th) | $K_{ATRP}$ (simul) | $c_{th}$ ($c'$ or $c''$) | $c_{simul}$ |
|---|---|---|---|---|---|---|---|
| 1 | 1.0 | $5 \times 10^4$ | 100/5 | $2.0 \times 10^{-5}$ | $1.97 \times 10^{-5}$ | 8.15 | *−134.5* |
| 2 | 1.0 | $5 \times 10^4$ | 5/5 | $2.0 \times 10^{-5}$ | $1.96 \times 10^{-5}$ | 66.5 | *−2370* |
| 3 | 1.0 | $5 \times 10^5$ | 100/5 | $2.0 \times 10^{-6}$ | $1.93 \times 10^{-6}$ | 8.15 | *5.46* |
| 4 | 1.0 | $5 \times 10^5$ | 5/5 | $2.0 \times 10^{-6}$ | $1.97 \times 10^{-6}$ | 66.5 | *62* |
| 5 | 1.0 | $5 \times 10^6$ | 100/5 | $2.0 \times 10^{-7}$ | $1.94 \times 10^{-7}$ | 8.15 | 8.15 |
| 6 | 1.0 | $5 \times 10^6$ | 5/5 | $2.0 \times 10^{-7}$ | $1.98 \times 10^{-7}$ | 66.5 | 66.5 |
| 7 | 1.0 | $5 \times 10^7$ | 100/5 | $2.0 \times 10^{-8}$ | $1.98 \times 10^{-8}$ | 8.15 | 8.15 |
| 8 | 1.0 | $5 \times 10^7$ | 5/5 | $2.0 \times 10^{-8}$ | $1.99 \times 10^{-8}$ | 66.5 | 66.5 |
| 9 | 1.0 | $5 \times 10^8$ | 100/5 | $2.0\times 10^{-9}$ | $1.99 \times 10^{-9}$ | 8.15 | 8.15 |
| 10 | 1.0 | $5 \times 10^8$ | 5/5 | $2.0 \times 10^{-9}$ | $1.99\times 10^{-9}$ | 66.5 | 66.5 |

[a] $c_{th}$ ($c'$ or $c''$) is the theoretical value of the intercept calculated using the expressions for $c'$ or $c''$ in eq 7 or 9, respectively. The numbers in italics are those that differ from the theoretically predicted values (cf. Appendix II).

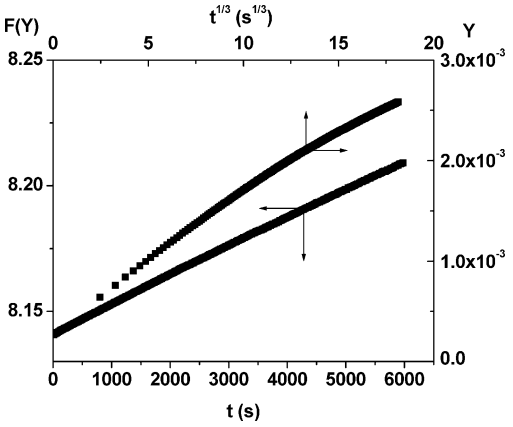


***Figure 7.*** Experiment for the determination of $K_{ATRP}$ via new equations ($F$(Y) vs $t$): $[Cu^IBr/PMDETA]_0 = 5$ mM, $[PEBr]_0 = 100$ mM, in MeCN at 22 °C (entry 4 in Table 4).

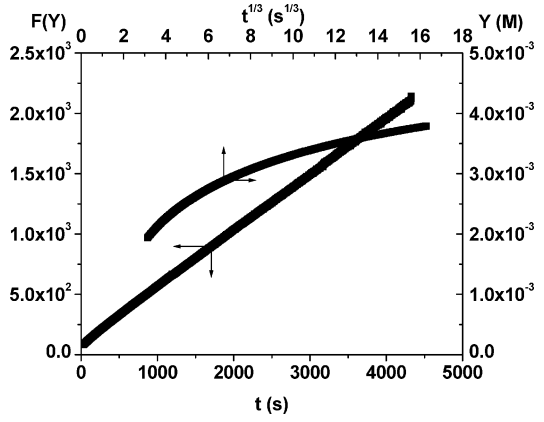


***Figure 8.*** Experiment for the determination of $K_{ATRP}$ via new equations ($F$(Y) vs $t$): $[Cu^IBr/TPMA]_0 = [EtBriB]_0 = 5$ mM, in MeCN at 22 °C (entry 7 in Table 4).

***Table 4.*** Experimental Determination of $K_{ATRP}$ via the New Equations[a]

| no. | ligand | $\lambda_{max}$ (nm) | initiator | $I_0/C_0$ (mM) | $c_{th}$ ($c'$ or $c''$) | $c_{exp}$ | $K_{ATRP}$ |
|---|---|---|---|---|---|---|---|
| 1 | bpy | 745 | EtBriB | 100/5 | 8.15 | 8.15 | $3.93 \times 10^{-9}$ |
| 2 | PMDETA | 745 | BrPN | 100/5 | 8.12 | 8.12 | $5.89 \times 10^{-7}$ |
| 3 | PMDETA | 745 | EtBriB | 100/5 | 8.15 | 8.15 | $7.46 \times 10^{-8}$ |
| 4 | PMDETA | 745 | PEBr | 100/5 | 8.15 | 8.14 | $3.27 \times 10^{-8}$ |
| 5 | PMDETA | 745 | PEBr | 10/10 | 33.4 | 33.4 | $3.68 \times 10^{-8}$ |
| 6 | PMDETA | 745 | MBrP | 100/5 | 8.15 | 8.15 | $3.95 \times 10^{-9}$ |
| 7 | TPMA | 985 | EtBriB | 5/5 | 66.5 | 66.5 | $9.65 \times 10^{-6}$ |
| 8 | TPMA | 985 | PEBr | 5/5 | 66.5 | 66.5 | $4.58 \times 10^{-6}$ |
| 9 | TPMA | 985 | PECl | 33.3/1.7 | 24.4 | 24.4 | $8.60 \times 10^{-7}$ |
| 10 | TPMA | 985 | BzBr | 100/5 | 8.15 | 8.15 | $6.78 \times 10^{-7}$ |
| 11 | TPMA | 985 | MBrP | 100/5 | 8.15 | 8.30 | $3.25 \times 10^{-7}$ |
| 12 | TPMA | 985 | MClP | 100/5 | 8.15 | 8.23 | $4.28 \times 10^{-8}$ |
| 13 | TPMA | 985 | MClP | 33.3/1.7 | 24.4 | 24.8 | $4.07 \times 10^{-8}$ |
| 14 | $Me_6$TREN | 985 | EtBriB | 5/5 | 66.5 | *−1250* | $1.54 \times 10^{-4}$ |
| 15[b] | PMDETA | | EtBriB | 1/20 | 40.7 | 40.7 | $6.06 \times 10^{-8}$ |

[a] $Cu^IBr$ was used for alkyl bromide, and $Cu^ICl$ was used for alkyl chloride initiators, respectively. Solvent = MeCN; temperature = 22 ± 2 °C. [b] Concentration of the initiator monitored by GC.

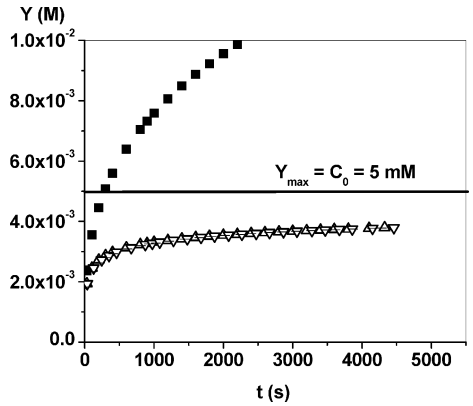


***Figure 9.*** Variation of Y vs $t$ for Y from experiment (△), from Fischer's equation (■), from the new equation (▽), and from simulation (- - -). [$Cu^I$-Br/TPMA]$_0$ = [EtBriB]$_0$ = 5 mM, in MeCN at 22 °C; $k_{act} = 62.4\ M^{-1}\ s^{-1}$, $K_{ATRP} = 9.65 \times 10^{-6}$, $k_t = 2.5 \times 10^9\ M^{-1}\ s^{-1}$ (entry 7 in Table 4). The solid line is drawn at the maximum possible value of Y, i.e., $Y_{max} = C_0$.

To check the validity of the newly derived equations over a range of conditions, experiments were carried out for $K_{ATRP}$ ranging from $\sim 10^{-9}$ to as high as $\sim 10^{-4}$ for both nonequimolar and equimolar reactions. When determining the $K_{ATRP}$ value, high conversion to X−$Cu^{II}$ may be reached. The concentration range of the $Cu^I$ species ($C_0$) is limited because of its relatively low solubility. Therefore, an excess of initiator ($I_0$) over the $Cu^I$ species was used for reactions with relatively small $K_{ATRP}$ (slow reactions) values, whereas equimolar concentrations of $I_0$ and $C_0$ were used for reactions with relatively large $K_{ATRP}$ (fast reactions) values. A typical plot for a reaction with an equimolar concentration of $I_0$ and $C_0$ is shown in Figure 8. The plot is straight with the intercept being identical to the expected one ($c_{exp} = 66.5$, $c_{th} = 66.5$), giving $K_{ATRP} = 9.65 \times 10^{-6}$. On the other hand, the plot with $Y \sim t^{1/3}$ shows a pronounced curvature. ($K_{ATRP}$ (initial) = $2.53 \times 10^{-6}$, $K_{ATRP}$ (final) = $1.38 \times 10^{-7}$, $K_{ATRP}$ (av) = $3.35 \times 10^{-7}$.) The values of $K_{ATRP}$ obtained for other nonequimolar and equimolar reaction systems are listed in Table 4 and discussed in the subsequent section.

To illustrate the excellent agreement of experimental data, simulations, and values calculated using the new eq 9, they were plotted in Figure 9 together with values calculated using the classic PRE eq 2. The value $k_{act} = 62.4\ M^{-1}\ s^{-1}$ was measured independently using the procedures published earlier;[21] the value $k_{deact} = 7.7 \times 10^5\ M^{-1}\ s^{-1}$ was calculated from $K_{ATRP}$ and $k_{act}$; and the value $k_t = 2.5 \times 10^9\ M^{-1}\ s^{-1}$ was based on a diffusion-controlled limit. The values of Y calculated from eq 9 perfectly overlapped with both the experimental and the simulated values. However, the values calculated from eq 2 (i.e., Fischer's equation) deviate strongly from the experimental values and even exceed the maximum possible values, $Y_{max} = C_0$. Thus, the newly derived eq 9 (as well as eq 8 for the nonequimolar case) can be successfully used for determination of $K_{ATRP}$ in ATRP. Fischer's eq 2 should not be used for the determination of $K_{ATRP}$, especially for systems with large values of $K_{ATRP}$.

**G. $K_{ATRP}$ Values for Various Catalysts and Initiators Measured by UV−Vis Spectrometry.** Using the aforementioned procedure, we studied various ATRP initiating/catalyst systems, and the corresponding equilibrium constants were determined in acetonitrile at 22 ± 2 °C. The results are summarized in Table 4. $K_{ATRP}$ ranges from very small values ($3.93 \times 10^{-9}$ for EtBriB with $Cu^IBr$/2bpy) to very large values ($1.54 \times 10^{-4}$ for EtBriB with $Cu^IBr$/$Me_6$TREN). As discussed before, the intercept values agree with predicted values, unless very large values of $K_{ATRP}$ are reached (e.g., entry 14).

The values of $K_{ATRP}$ reported in Table 4 illustrate the strong effect of ligand, halogen, and alkyl groups. For example, values of $K_{ATRP}$ for EtBriB increase from $3.93 \times 10^{-9}$ for $Cu^IBr$/2bpy (entry 1 in Table 4) to $7.46 \times 10^{-8}$ for $Cu^IBr$/PMDETA (entry 3 in Table 4), to $9.65 \times 10^{-6}$ for $Cu^IBr$/TMPA (entry 7 in Table 4), and to $1.54 \times 10^{-4}$ for $Cu^IBr$/$Me_6$TREN (entry 14 in Table 4). Thus, the relative activity of the catalysts derived from the ligands increases in the order bpy (1) < PMDETA (20) < TPMA (2500) < $Me_6$TREN (40 000). These results are in very good agreement with previous measurements and estimates.[19,40,41]

Three structural features of alkyl halides affect their reactivities and equilibrium constants. Generally, tertiary alkyl halides are more active than secondary alkyl halides, which are more active than primary alkyl halides. Indeed, the $K_{ATRP}$ value for EtBriB (entry 3 in Table 4) is 20-fold larger than that for MBrP (entry 6 in Table 4) when $Cu^IBr$/PMDETA is used as the catalyst and is 30-fold larger than that with $Cu^IBr$/TPMA (entries 7 and 11 in Table 4). The $K_{ATRP}$ value for PEBr (entry 8 in Table 4) is 7 times larger than that for BzBr (entry 10 in Table 4) with $Cu^IBr$/TPMA as the catalyst.

Another important parameter is the nature of the radical stabilizing group. The most stabilizing is the nitrile group, followed by the phenyl and then by the ester groups. Thus, the $K_{ATRP}$ value for secondary BrPN (entry 2 in Table 4) is 18 times higher than that for PEBr (entry 4 in Table 4) which is in turn 8 times higher than that for MBrP (entry 6 in Table 4) using $Cu^IBr$/PMDETA. A similar trend is observed for the TPMA-based catalyst. These results are in good agreement with DFT calculations of BDEs of various ATRP initiators.[42]

The third important parameter affecting $K_{ATRP}$ is the halogen. Values of $K_{ATRP}$ for R−Br are 6 to 10 times larger than those

(40) Gobelt, B.; Matyjaszewski, K. *Macromol. Chem. Phys.* **2000**, *201*, 1619−1624.
(41) Qiu, J.; Matyjaszewski, K.; Thouin, L.; Amatore, C. *Macromol. Chem. Phys.* **2000**, *201*, 1625−1631.
(42) Gillies, M. B.; Matyjaszewski, K.; Norrby, P.-O.; Pintauer, T.; Poli, R.; Richard, P. *Macromolecules* **2003**, *36*, 8551−8559.

for Cl-based systems (entry 8 vs entry 9 and entry 11 vs entry 12 in Table 4). These differences indicate that the C−Br bond is relatively weaker than the C−Cl bond in comparison to the Cu−Br and Cu−Cl bonds. These results are also in good agreement with previously reported values of $K_{ATRP}$ for styrene polymerization at higher temperatures.[23]

We are currently studying rate constants of activation for the same ATRP systems and will be able to calculate rate constants of deactivation and reach a deeper insight into ATRP systems. This will allow the correlation of structures of the involved reagents with the reactivities in both activation and deactivation processes.

Values of $K_{ATRP}$ reported in Table 4 also indicate that they are not sensitive to the ratio of reagents (entry 4 vs 5 and entry 12 vs 13 in Table 4). Variations in the ratio provide similar $K_{ATRP}$ values, and even reversing the excess of the initiator over the catalyst (entry 15 vs 4 in Table 4) still gives the same values of $K_{ATRP}$. The former was measured using GC rather than UV−vis spectrometry and required some adjustment of the derived equation (vide infra).

**H. Evaluation of the Validity of the New Equations for Determination of $K_{ATRP}$ by GC ($C_0 > I_0$).** Analogous to the procedure of following the concentration of the X−Cu$^{II}$ species (Y) by UV−vis spectrometry, one can monitor the initiator concentration ($I$) by other analytical techniques such as GC, NMR, HPLC, etc. Similar equations can be obtained by substituting $Y = I_0 - I$ into eq 7.

For $C_0 \neq I_0$

$$\left(\frac{I_0C_0}{C_0 - I_0}\right)^2\left(\frac{1}{C_0{}^2I} + \frac{2}{I_0C_0(C_0 - I_0)}\ln\left(\frac{I}{C_0 + I - I_0}\right) + \frac{1}{I_0{}^2(C_0 + I - I_0)}\right) = 2k_tK_{ATRP}^2t + c'$$

$$\text{where } c' = \left(\frac{I_0C_0}{C_0 - I_0}\right)^2\left(\frac{1}{C_0{}^2I_0} + \frac{2}{I_0C_0(C_0 - I_0)}\ln\frac{I_0}{C_0} + \frac{1}{I_0{}^2C_0}\right) \quad (11)$$

Figure 10 shows a plot used for the determination of $K_{ATRP}$ following the concentration of the initiator by GC, where

$$F(I) = \left(\frac{I_0C_0}{C_0 - I_0}\right)^2\left(\frac{1}{C_0{}^2I} + \frac{2}{I_0C_0(C_0 - I_0)}\ln\left(\frac{I}{C_0 + I - I_0}\right) + \frac{1}{I_0{}^2(C_0 + I - I_0)}\right) \quad (12)$$

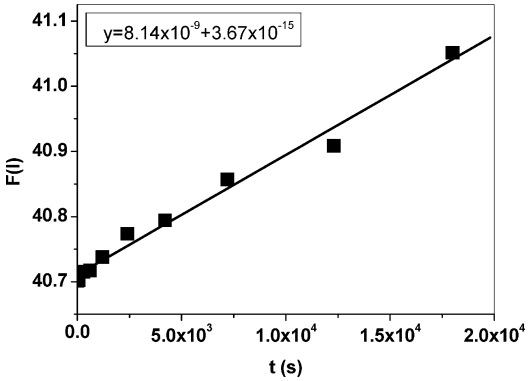


***Figure 10.*** Experimental determination of $K_{ATRP}$ using GC via eq 12 ($F(I)$ vs $t$): $[Cu^IBr/PMDETA]_0 = 20$ mM, $[EtBriB]_0 = 1$ mM, in MeCN at 22 °C (entry 15 in Table 4).

The plot is a straight line, and the calculated value of $K_{ATRP}$ ($6.06 \times 10^{-8}$, entry 15 in Table 4) is comparable to that obtained by using UV−vis spectrometry ($7.46 \times 10^{-8}$, entry 3 in Table 4). GC (or NMR) may have some advantages over UV−vis spectrometry because all products of the reactions can be independently analyzed.

## Conclusions

New equations were derived for the evolution of the persistent radical (Y) over time for both nonequimolar and equimolar ATRP reactions. From these new equations, $K_{ATRP}$ values were obtained for several ATRP systems using UV−vis spectrometric or GC measurements. Fischer's original equations for the persistent radical effect could be used only for a low amount of persistent radical formation and consequently for systems with relatively low $K_{ATRP}$ values. For higher conversion and for more reactive systems, significant deviations from linearity in $t^{1/3}$ plots are observed. The same methodology can be applied to NMP and other systems controlled by the persistent radical effect. In a forthcoming paper, we will analyze in more detail the kinetics and peculiarities of such systems.

**Acknowledgment.** This paper is dedicated to the memory of Prof. Hanns Fischer who passed away on February 22, 2005. The financial support from the National Science Foundation (CHE 04-05627 and DMR 05-49353) and CRP Consortium at Carnegie Mellon University is gratefully acknowledged. Helpful discussions with Wade Braunecker are acknowledged. Constructive suggestions by Prof. Takeshi Fukuda are gratefully appreciated.

**Supporting Information Available:** Description of the time range applicable for Fischer's equations, detailed derivation of the new equations, and deviations for systems with slow deactivation. This material is available free of charge via the Internet at http://pubs.acs.org.

JA0558591